

Effect of sweep angle on bifurcation analysis of a wing containing cubic nonlinearity

Saied Irani^a, Mohammadreza Amoozgar^{*} and Hamid Sarrafzadeh^b

Department of Aerospace Engineering, Khaje Nasir Toosi University of Technology, Tehran, Iran

(Received September 6, 2015, Revised June 8, 2016, Accepted June 10, 2016)

Abstract. Limit cycle oscillations (LCO) as well as nonlinear aeroelastic analysis of a swept aircraft wing with cubic restoring moments in the pitch degree of freedom is investigated. The unsteady aerodynamic loading applied on the wing is modeled by using the strip theory. The harmonic balance method is used to calculate the LCO frequency and amplitude for the swept wing. Finally the super and subcritical Hopf bifurcation diagrams are plotted. It is concluded that the type of bifurcation and turning point location is sensitive to the system parameters such as wing geometry and sweep angle.

Keywords: cubic nonlinearity; bifurcation; limit cycle oscillations (LCO); harmonic balance method; sweep angle

1. Introduction

Interaction of aerodynamic, elasticity and dynamics is called aeroelasticity, and many disciplines in this field such as dynamic instability and flutter, are investigated by many researchers. The aeroelastic results under the assumption of structural linearity, may disagree with the physical phenomena as most real structures may have structural nonlinearities such as freeplay, bilinear, cubic non-linearity, friction, and hysteresis.

Limit cycle oscillations (LCOs) and bifurcations arising from a concentrated structural nonlinearity in the restoring forces were first studied by Woolston *et al.* (1957) and Shen (1977). Breitbach (1979) described the flutter analysis of an airplane with multiple structural nonlinearities in the control system. Laurenson (1980) studied flutter of a missile control surface with freeplay using the describing function method. Lee and Torn (1989) applied the describing function method to analyze the flutter characteristics of the F-18 aircraft. They considered a nonlinearity of the type represented by a bilinear spring at the wing-fold hinge. They also considered free-play nonlinearity at the leading edge flap. Tang and Dowell (1992) investigated free-play nonlinearity in the pitch degree of freedom. It was shown that free-play nonlinearities introduced limit cycle oscillations at speeds below the linear flutter speed.

They concluded that the amplitude of limit cycle oscillations depended on initial conditions,

^{*}Corresponding author, MSc. Graduated, E-mail: Amoozgar@sina.kntu.ac.ir

^aAssociate Professor, E-mail: Irani@kntu.ac.ir

^bMSc. Graduated, E-mail: Sarrafzadeh@sina.kntu.ac.ir

airspeed, and degree of nonlinearity. Kim and Lee (1996), particularly investigated same problem but with a flexible two degrees of freedom airfoil. They performed nonlinear aeroelastic analyses for both the frequency domain and time domain.

The nonlinear response of a structurally nonlinear airfoil in subsonic flow has similarly been the subject of a number of investigations such as works done by Conner *et al.* (1998) and Tang *et al.* (1998) for discontinuous structural nonlinearities, and by O'Neil (1998) and Sheta *et al.* (2002) for continuous structural nonlinearities. Sedaghat *et al.* (2001) considered the estimation of the hopf bifurcation point for aeroelastic systems. In this investigation, a procedure was developed to produce and solve algebraic equations for any aeroelastic systems, with and without frequency-dependent aerodynamics, to predict the hopf bifurcation point. Dessi *et al.* (2002) studied the limit-cycle stability reversal near a hopf bifurcation with aeroelastic applications. In this investigation numerical studies were performed to show the dependence of the Hopf bifurcation characteristics upon the structural and geometric properties of the wing section. Dessi and Mastroddi (2004) constructed a theoretical model with a three-degree-of-freedom aeroelastic typical section with a trailing-edge control surface including cubic nonlinear springs for both the nonlinear description of the torsional stiffness and of the hinge elastic moment. The equations of motion are then analyzed by a singular perturbation technique based on the normal-form method.

Experimental investigation of the aeroelastic response of a wing section with a structural freeplay nonlinearity were performed by Marsden *et al.* (2005). They concluded that the friction damping in the experimental apparatus, particularly in the plunge degree of freedom is not negligible, and is probably responsible for the damped LCO behavior. Liu *et al.* (2007) developed a high dimensional harmonic balance approach for an aeroelastic airfoil with cubic restoring forces. In this research a new formulation of the harmonic balance method was employed for the aeroelastic airfoil to investigate the amplitude and frequency of the limit cycle oscillations. Limit cycle oscillation of rectangular cantilever wings containing cubic nonlinearity in an incompressible flow has been studied by Ghadiri and Razi (2007). In this study the nonlinear aeroelastic behavior of the 2DOF rectangular cantilever wing with hardening and softening cubic nonlinearities was studied in the time domain, and the prediction of LCO amplitude and frequency via the HB method and numerical solution was investigated.

Irani *et al.* (2011), studied the Bifurcation in a 3-DOF Airfoil with Cubic Structural Nonlinearity. They showed that the type of bifurcation and turning point location depends on the characteristics of the airfoil as well as the parameters of structural nonlinearity. Numerical investigation of the effects of structural geometric and material nonlinearities on limit-cycle oscillation of a cropped delta wing was considered by Peng *et al.* (2011). This study demonstrated that the LCO of the cropped delta wing was not only closely related to geometric nonlinearity, but was also remarkably affected by material nonlinearity. Numerical bifurcation analysis of static stall of airfoil and dynamic stall under unsteady perturbation was studied by Liu *et al.* (2012). In this research the static and dynamic stalls were studied from viewpoint of nonlinear dynamics and it was concluded that the oscillating airfoil could have a positive influence on the aerodynamic performance of airfoil by modifying the streamline topology. Anton *et al.* (2012) analyzed the hopf bifurcation of an aeroelastic model using stochastic normal form. In this research, the effects of parameter uncertainties on the dynamical response of an aeroelastic model representing an oscillating airfoil in pitch and plunge with linear aerodynamics and cubic structural nonlinearities were investigated.

Harmonic Balance Method is used to determine the turning point location respect to the free-stream flow velocity and it is an efficient method to illustrate unstable LCOs before the Hopf

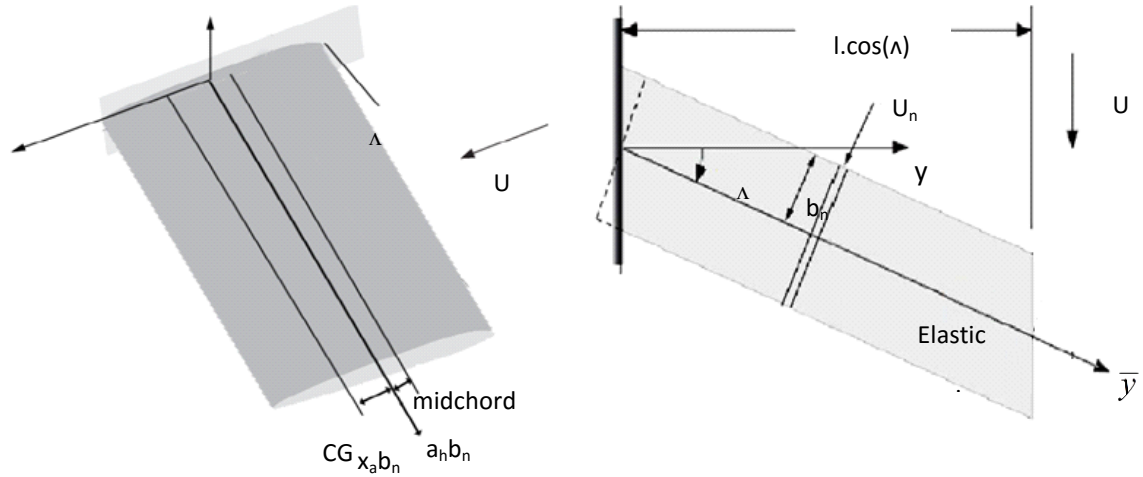


Fig. 1 Swept wing configuration

point, which is in this case is equal to the linear flutter speed.

Cubic nonlinearity in the pitch degree of freedom causes subcritical knee-like and supercritical pitchfork-like shape Hopf bifurcation respect to the characteristics of the wing. More recently, Eken and Kaya (2015) investigated the limit cycle oscillation of swept cantilever wings containing cubic nonlinearity. They showed that the sweep angle can affect the wing response dramatically.

It seems that the effect of wing sweep angle on bifurcation analysis of swept wings has not received much attention in the literature. So in the current study, the effects of wing sweep angle on bifurcation analysis are presented.

2. Governing equations

A swept cantilever wing modeled as a classic beam containing two degree of freedom as shown in Fig. 1, is considered. By using standard notation, the plunge deflection and pitch angle are denoted here by h , positive in downward direction, and α , positive nose up, respectively. The elastic axis distance from the mid-chord is $a_h b_n$, where b is the semi-chord length, while the distance between the wing center of gravity and the elastic axis is $x_a b_n$. All distances are positive when measured towards the TE of the wing.

The kinetic energy, the potential energy and the virtual work of aerodynamic forces acting on the wing may be expressed as follows

$$\begin{aligned}
 T &= \frac{1}{2} \int_0^l \left[m(\dot{h} + b_n x_a \dot{\alpha})^2 + I_\alpha \dot{\alpha}^2 \right] d\bar{y}, \\
 V &= \frac{1}{2} \int_0^l \left[EI \left(\frac{\partial^2 h}{\partial y^2} \right)^2 + GJ \left(\frac{\partial \alpha}{\partial y} \right)^2 \right] d\bar{y}, \\
 \delta W_A &= \int_0^l (L \delta w + M \delta \theta) dx.
 \end{aligned} \tag{1}$$

Where m , I_a , EI , GJ , L and M are wing mass per unit length, wing mass moment of inertia per unit length about wing center of gravity, bending stiffness, torsional stiffness and the aerodynamic lift and moment, respectively. By considering the procedure of Ghadiri *et al.* (2007), the following aeroelastic equations can be obtained

$$\begin{aligned} A_5(lm\ddot{h}_1) + A_7(lmb_n x_\alpha \ddot{\alpha}_1) + A_3\left(\frac{EI}{l^3} h_1\right) &= Q_h, \\ A_6 lm(b_n x_\alpha)^2 \ddot{\alpha}_1 + A_7(lmb_n x_\alpha \ddot{h}_1) + lA_6 I_\alpha \ddot{\alpha}_1 + A_4\left(\frac{GJ}{l} \alpha_1\right) &= Q_\alpha. \end{aligned} \quad (2)$$

The coefficients A_1, A_2, A_3, \dots are the integration of the selected mode shapes of the wing and are defined in Appendix A.

The non-dimensional parameters are considered as below:

$$\xi = \frac{h}{b_n}, \quad r_a = \sqrt{\frac{I_a}{mb^2}}, \quad \mu = \frac{m}{\rho\pi b_n^2}, \quad \bar{\omega} = \frac{\omega_\xi}{\omega_\alpha}, \quad U_n^* = \frac{U_n}{b_n \omega_\alpha}, \quad \eta = \frac{\bar{y}}{l}, \quad \tau = \frac{U_n t}{b_n}.$$

By substituting the dimensionless parameters into Eq. (2), the final form of governing equations can be written as follow

$$\begin{aligned} A_5 \xi_1'' + A_7 (x_\alpha \alpha_1'') + A_5 \left(\frac{\bar{\omega}}{U_n^*}\right)^2 G(\xi_1) &= \frac{b_n}{mU_n^2 l} Q_h, \\ A_7 \left(\frac{x_\alpha}{r_a^2} \xi_1''\right) + A_6 \alpha_1'' + A_6 \left(\frac{1}{U_n^*}\right)^2 M(\alpha_1) &= \frac{b_n^2}{I_a U_n^2 l} Q_\alpha. \end{aligned} \quad (3)$$

The aerodynamic lift and moment used in this paper are the unsteady aerodynamic loading based on strip theory like the model used in Hadadpour *et al.* (2008), and in dimensionless form are

$$\begin{aligned} L(\xi, \alpha) &= \rho U_n^{*2} b_n^3 \omega_\alpha^2 \pi [(\alpha' + \xi'' + \frac{2b_n}{l} \frac{\partial \xi'}{\partial \eta} \tan \Lambda + \frac{b_n}{l} \frac{\partial \alpha}{\partial \eta} \tan \Lambda + (\frac{b_n}{l})^2 \frac{\partial^2 \xi'}{\partial \eta^2} \tan^2 \Lambda) - \\ &- a_h (\alpha'' + \frac{2b_n}{l} \frac{\partial \alpha'}{\partial \eta} \tan \Lambda + (\frac{b_n}{l})^2 \frac{\partial^2 \alpha}{\partial \eta^2} \tan^2 \Lambda) + 2W_{3/4}(\tau)], \\ M(\xi, \alpha) &= \rho U_n^{*2} b_n^4 \omega_\alpha^2 \pi [-(0.5 - a_h) \alpha' + \frac{b_n}{2l} \frac{\partial \alpha}{\partial \eta} \tan \Lambda + a_h (\xi'' + \frac{2b_n}{l} \frac{\partial \xi'}{\partial \eta} \tan \Lambda + \frac{b_n}{l} \frac{\partial \alpha}{\partial \eta} \tan \Lambda \\ &+ (\frac{b_n}{l})^2 \frac{\partial^2 \xi}{\partial \eta^2} \tan^2 \Lambda) - (\frac{1}{8} + a_h^2) (\alpha'' + \frac{2b_n}{l} \frac{\partial \alpha'}{\partial \eta} \tan \Lambda + (\frac{b_n}{l})^2 \frac{\partial^2 \alpha}{\partial \eta^2} \tan^2 \Lambda) + 2(0.5 + a_h) W_{3/4}(\tau)]. \end{aligned} \quad (4)$$

Where, Λ is the wing sweep angle, and $W_{3/4}$ in terms of Wagner's function can be written as follow

$$\begin{aligned} W_{3/4}(\tau) &= (\alpha(0) + \xi'(0) + (0.5 - a_h) \alpha'(0) + \frac{b_n}{l} (0.5 - a_h) \frac{\partial \alpha(0)}{\partial \eta} \tan \Lambda + \frac{b_n}{l} \frac{\partial \xi(0)}{\partial \eta} \tan \Lambda) \varphi(\tau) + \\ &+ \int_0^\tau \varphi(\tau - \sigma) (\xi''(\sigma) + \alpha'(\sigma) + (0.5 - a_h) \alpha''(\sigma) + \frac{b_n}{l} \frac{\partial \xi'(\sigma)}{\partial \eta} \tan \Lambda + \frac{b_n}{l} (0.5 - a_h) \frac{\partial \alpha'(\sigma)}{\partial \eta} \tan \Lambda) d\sigma \end{aligned} \quad (5)$$

In Eq. (5), $\varphi(\tau)$ is Wagner function and can be determined approximately by using the following expression:

$$\varphi(\tau) = (1 - \psi_1 e^{-\varepsilon_1 \tau} - \psi_2 e^{-\varepsilon_2 \tau}).$$

where the constants $\psi_1=0.165$, $\varepsilon_1=0.0455$, $\psi_2=0.335$, and $\varepsilon_2=0.3$ are borrowed from Jones R.T (1940).

Due to the existence of the integral terms in the integro-differential Eq.(5), it is cumbersome to integrate them numerically. A simpler set of equations was derived by Lee *et al.* (1997), and they introduced four new variables as

$$\begin{cases} w_1 = \int_0^\tau e^{-\varepsilon_1(\tau-\sigma)} \xi(\sigma) d\sigma \Rightarrow w_1' = \xi(\tau) - \varepsilon_1 w_1 \\ w_2 = \int_0^\tau e^{-\varepsilon_2(\tau-\sigma)} \xi(\sigma) d\sigma \Rightarrow w_2' = \xi(\tau) - \varepsilon_2 w_2 \\ w_3 = \int_0^\tau e^{-\varepsilon_1(\tau-\sigma)} \alpha(\sigma) d\sigma \Rightarrow w_3' = \alpha(\tau) - \varepsilon_1 w_3 \\ w_4 = \int_0^\tau e^{-\varepsilon_2(\tau-\sigma)} \alpha(\sigma) d\sigma \Rightarrow w_4' = \alpha(\tau) - \varepsilon_2 w_4 \end{cases} \quad (6)$$

By integrating and employing the above variables, the complete aeroelastic equation of motion can be obtained as

$$\begin{aligned} & A_5 \xi_1'' + A_7 (x_a \alpha_1'') + A_5 \left(\frac{\bar{\omega}}{U_n^*} \right)^2 G(\xi_1) + \frac{1}{\mu} [\xi_1'' A_5 - a_h \alpha_1'' A_7 + 2(\psi_1 \varepsilon_1 + \psi_2 \varepsilon_2) \xi_1' A_5 + 2(1 - \psi_1 - \psi_2) \xi_1' A_5 + \\ & + 2((1 - \psi_1 - \psi_2) + (0.5 - a_h)(\psi_1 \varepsilon_1 + \psi_2 \varepsilon_2)) \alpha_1' A_7 + (1 + 2(0.5 - a_h)(1 - \psi_1 - \psi_2)) \alpha_1' A_7 + \\ & + \frac{2b_n \tan \Lambda}{l} (1 - \psi_1 - \psi_2) \xi_1 A_8 + \frac{2b_n \tan \Lambda}{l} \xi_1' A_8 + \frac{b_n \tan \Lambda}{l} (1 + 2(0.5 - a_h)(1 - \psi_1 - \psi_2)) \alpha_1 A_9 - \\ & - \frac{2b_n \tan \Lambda}{l} a_h \alpha_1' A_9 + \left(\frac{b_n \tan \Lambda}{l} \right)^2 \xi_1 A_{12} - a_h \left(\frac{b_n \tan \Lambda}{l} \right)^2 \alpha_1 A_{13} - 2\psi_1 \varepsilon_1^2 w_1 A_5 - 2\psi_2 \varepsilon_2^2 w_2 A_5 + \\ & + 2\psi_1 \varepsilon_1 (1 - (0.5 - a_h) \varepsilon_1) w_3 A_7 + 2\psi_2 \varepsilon_2 (1 - (0.5 - a_h) \varepsilon_2) w_4 A_7 + \frac{2b_n \tan \Lambda}{l} \psi_1 \varepsilon_1 w_1 A_8 + \\ & + \frac{2b_n \tan \Lambda}{l} \psi_2 \varepsilon_2 w_2 A_8 + \frac{2b_n \tan \Lambda}{l} \psi_1 \varepsilon_1 (0.5 - a_h) w_3 A_9 + \frac{2b_n \tan \Lambda}{l} \psi_2 \varepsilon_2 (0.5 - a_h) w_4 A_9 - \\ & - 2(\xi_1(0) A_5 + (0.5 - a_h) \alpha_1(0) A_7) (\psi_1 \varepsilon_1 e^{-\varepsilon_1 \tau} + \psi_2 \varepsilon_2 e^{-\varepsilon_2 \tau})] = 0, \\ & A_7 \left(\frac{x_a}{r_a^2} \xi_1'' \right) + A_6 \alpha_1'' + A_6 \left(\frac{1}{U_n^*} \right)^2 M(\alpha_1) - \frac{1}{\mu r_a^2} [a_h \xi_1'' A_7 + (1 + 2a_h)(\psi_1 \varepsilon_1 + \psi_2 \varepsilon_2) \xi_1' A_7 + \\ & + (1 + 2a_h)(1 - \psi_1 - \psi_2) \xi_1' A_7 + (1 + 2a_h)((1 - \psi_1 - \psi_2) + (0.5 - a_h)(\psi_1 \varepsilon_1 + \psi_2 \varepsilon_2)) \alpha_1' A_6 - \\ & - (0.5 - a_h)(1 - (1 + 2a_h)(1 - \psi_1 - \psi_2)) \alpha_1' A_6 + (1 + 2a_h) \frac{b_n \tan \Lambda}{l} (1 - \psi_1 - \psi_2) \xi_1 A_{10} + \\ & + \frac{b_n \tan \Lambda}{l} (a_h + (1 + 2a_h)(0.5 - a_h)(1 - \psi_1 - \psi_2)) \alpha_1 A_{11} - \frac{2b_n \tan \Lambda}{l} \left(\frac{1}{8} + a_h^2 \right) \alpha_1' A_{11} - \\ & - \left(\frac{1}{8} + a_h^2 \right) \left(\frac{b_n \tan \Lambda}{l} \right)^2 \alpha_1 A_{15} - (1 + 2a_h) \psi_1 \varepsilon_1^2 w_1 A_7 - (1 + 2a_h) \psi_2 \varepsilon_2^2 w_2 A_7 - \left(\frac{1}{8} + a_h^2 \right) \alpha_1'' A_6 + \end{aligned}$$

$$\begin{aligned}
& +(1+2a_h)\psi_1\varepsilon_1(1-(0.5+a_h)\varepsilon_1)w_3A_6 + (1+2a_h)\psi_2\varepsilon_2(1-(0.5+a_h)\varepsilon_2)w_4A_6 + \\
& + \frac{b_n \tan \Lambda}{l} \psi_1\varepsilon_1(1+2a_h)w_1A_{10} + \frac{b_n \tan \Lambda}{l} \psi_1\varepsilon_1(1+2a_h)(0.5-a_h)w_3A_{11} + \\
& + \frac{b_n \tan \Lambda}{l} \psi_2\varepsilon_2(1+2a_h)(0.5-a_h)w_4A_{11} + a_h \left(\frac{b_n \tan \Lambda}{l}\right)^2 \xi_1 A_{14} + \frac{b_n \tan \Lambda}{l} \psi_2\varepsilon_2(1+2a_h)w_2A_{10} - \\
& -(1+2a_h)(\xi_1(0)A_7 + (0.5-a_h)\alpha_1(0)A_6)(\psi_1\varepsilon_1e^{-\varepsilon_1\tau} + \psi_2\varepsilon_2e^{-\varepsilon_2\tau}) + a_h \frac{2b_n \tan \Lambda}{l} \xi_1' A_{10}] = 0.
\end{aligned} \tag{7}$$

By summarizing the above equations, the aeroelastic equations of motion can be written as:

$$\begin{aligned}
c_a \xi_1'' + c_b \alpha_1'' + c_1 \xi_1 + c_2 \xi_1' + c_3 \alpha_1 + c_4 \alpha_1' + c_5 w_1 + c_6 w_2 + c_7 w_3 + c_8 w_4 + A_5 \left(\frac{\bar{\omega}}{U_n^*}\right)^2 G(\xi) &= f(\tau), \\
d_a \xi_1'' + d_b \alpha_1'' + d_1 \xi_1 + d_2 \xi_1' + d_3 \alpha_1 + d_4 \alpha_1' + d_5 w_1 + d_6 w_2 + d_7 w_3 + d_8 w_4 + A_6 \left(\frac{1}{U_n^*}\right)^2 M(\alpha) &= g(\tau).
\end{aligned} \tag{8}$$

Where c_i and d_i ($i=a,b$) and c_j and d_j ($j=1,2,\dots,8$) are given in Appendix B. the expressions for $f(\tau)$ and $g(\tau)$ are

$$\begin{aligned}
f(\tau) &= \frac{2}{\mu} \left[(\psi_1\varepsilon_1e^{-\varepsilon_1\tau} + \psi_2\varepsilon_2e^{-\varepsilon_2\tau}) \left(A_5 \xi_1(0) + A_7 \left(\frac{1}{2} - a_h\right) \alpha_1(0) \right) \right], \\
g(\tau) &= - \left(\frac{1+2a_h}{\mu r_a^2} \right) \left[(\psi_1\varepsilon_1e^{-\varepsilon_1\tau} + \psi_2\varepsilon_2e^{-\varepsilon_2\tau}) \left(A_7 \xi_1(0) + A_6 \left(\frac{1}{2} - a_h\right) \alpha_1(0) \right) \right].
\end{aligned} \tag{9}$$

The nonlinear stiffness terms for the cubic nonlinearity are defined as follow

$$G(\xi) = \beta_\xi \xi + \beta_{\xi^3} \xi^3, \quad M(\alpha) = \beta_\alpha \alpha + \beta_{\alpha^3} \alpha^3. \tag{10}$$

3. Numerical simulation

The governing aeroelastic equations in the time domain, Eq. (8), can easily be rewritten as a set of first order ordinary differential equations (ODEs). By a suitable transformation, the resulting set of eight ODEs is given as follows

$$\frac{dX}{d\tau} = F(X, \tau) \tag{11}$$

By assuming the following variables:

$$x_1 = \xi, x_2 = \xi', x_3 = \alpha, x_4 = \alpha', x_5 = w_1, x_6 = w_2, x_7 = w_3, x_8 = w_4.$$

vector X takes the following form

$$X = [x_2 \ x_4 \ x_1 \ x_3 \ x_5 \ x_6 \ x_7 \ x_8]^T \tag{12}$$

The initial conditions of the system can be expressed as

$$\mathbf{X}(0) = [\xi'(0) \quad \alpha_1'(0) \quad \xi_1(0) \quad \alpha_1(0) \quad 0 \quad 0 \quad 0 \quad 0]^T$$

The first ODEs in the state space form are given as

$$\begin{aligned} x_1' &= x_2, \quad x_2' = \frac{c_0 H - d_0 P}{d_0 c_1 - c_0 d_1}, \quad x_3' = x_4, \quad x_4' = \frac{-c_1 H + d_1 P}{d_0 c_1 - c_0 d_1}, \\ x_5' &= x_1 - \varepsilon_1 x_5, \quad x_6' = x_1 - \varepsilon_2 x_6, \quad x_7' = x_3 - \varepsilon_1 x_7, \quad x_8' = x_3 - \varepsilon_2 x_8 \end{aligned} \tag{13}$$

Where

$$\begin{aligned} P &= c_1 x_1 + c_2 x_2 + c_3 x_3 + c_4 x_4 + c_5 x_5 + c_6 x_6 + c_7 x_7 + c_8 x_8 + A_5 \frac{\bar{\omega}^2}{U_n^{*2}} G(x_1) - f(\tau), \\ Q &= d_1 x_1 + d_2 x_2 + d_3 x_3 + d_4 x_4 + d_5 x_5 + d_6 x_6 + d_7 x_7 + d_8 x_8 + A_6 \frac{1}{U_n^{*2}} M_a(x_3) - g(\tau). \end{aligned} \tag{14}$$

The standard fourth-order Runge-Kutta method is used to integrate the system of Eq.(11) under given initial conditions as mentioned.

4. Computing linear flutter speed

Substituting $G(\zeta)=\zeta$ and $M(\alpha)=\alpha$ into Eq. (8) yields

$$\mathbf{X}' = \mathbf{A}^{-1} \mathbf{F} - \mathbf{A}^{-1} \mathbf{B} \mathbf{X} \tag{15}$$

where \mathbf{A} , \mathbf{B} are 8 by 8 and \mathbf{F} is 8 by 1 sparse matrices given as follow

$$\mathbf{A} = \begin{bmatrix} c_a & c_b & 0 & 0 & 0 & 0 & 0 & 0 \\ d_a & d_b & 0 & 0 & 0 & 0 & 0 & 0 \\ 0 & 0 & 1 & 0 & 0 & 0 & 0 & 0 \\ 0 & 0 & 0 & 1 & 0 & 0 & 0 & 0 \\ 0 & 0 & 0 & 0 & 1 & 0 & 0 & 0 \\ 0 & 0 & 0 & 0 & 0 & 1 & 0 & 0 \\ 0 & 0 & 0 & 0 & 0 & 0 & 1 & 0 \\ 0 & 0 & 0 & 0 & 0 & 0 & 0 & 1 \end{bmatrix}, \quad \mathbf{B} = \begin{bmatrix} c_2 & c_4 & c_1 + A_5 \frac{\bar{\omega}^2}{U_n^{*2}} & c_3 & c_5 & c_6 & c_7 & c_8 \\ d_2 & d_4 & d_1 & d_3 + A_6 \frac{1}{U_n^{*2}} & d_5 & d_6 & d_7 & d_8 \\ -1 & 0 & 0 & 0 & 0 & 0 & 0 & 0 \\ 0 & -1 & 0 & 0 & 0 & 0 & 0 & 0 \\ 0 & 0 & -1 & 0 & \varepsilon_1 & 0 & 0 & 0 \\ 0 & 0 & -1 & 0 & 0 & \varepsilon_2 & 0 & 0 \\ 0 & 0 & 0 & -1 & 0 & 0 & \varepsilon_1 & 0 \\ 0 & 0 & 0 & -1 & 0 & 0 & 0 & \varepsilon_2 \end{bmatrix} \tag{15}$$

$$\mathbf{F} = [f(\tau) \quad g(\tau) \quad 0 \quad 0 \quad 0 \quad 0 \quad 0 \quad 0]^T.$$

The linear flutter velocity U_L^* is obtained by solving the resultant eigenvalue problem. Stability of the linear system depends on the eigenvalues of $-\mathbf{A}^{-1} \mathbf{B}$ in Eq. (15). To obtain the solution to the problem, the eigenvalues and eigenvectors of the system must be determined. The real parts of the eigenvalues represent the damping and the imaginary parts represent the frequency. In order to find the aeroelastic instability, one can use the plot of damping against speed and the corresponding airspeed with zero damping is called the flutter or divergence speed.

Table 1 Case studies of the linear analysis: physical, geometrical and nondimensional characteristics

Model	Λ (deg)	f_h (cps)	f_a (cps)	l (in)	b_n (ft)	a_h	x_a	r_a^2	μ
30B-2	30	12.1	88.8	24.8	0.167	-0.2	0.12	0.277	37.7
40A-5	15	9.3	88.2	24.8	0.167	-0.2	0.12	0.277	35.1
50A-2	-15	15	137	24.8	0.167	-0.34	0.34	0.352	8
93-3	30	6.3	50	23.6	0.167	-0.12	0.24	0.428	73.2
85-3	60	5	63	44	0.167	-0.36	0.38	0.378	34.5
30D-1	15	13.2	82.4	24.8	0.167	-0.21	0.17	0.28	8.7

Table 2 Validation of sweep effect on instability speed.

Model	$U_{flutter}$ m/s	$U_{divergence}$ m/s	$U_{instability}$ m/s Experimental	$\Lambda_{first\ flutter}$	Type of instability	Error %
30B-2	103.906	118.48	105.050	-3.5	Flutter	1.089005
40A-5	93.292	113.552	89.852	-2	Flutter	-3.82852
50A-2	84.437	45.006	46.938	-3.2	Divergence	4.116068
93-3	81.789	165.664	82.701	-3.6	Flutter	1.102768
85-3	132.726	332.558	135.450	-4	Flutter	2.011074
30D-1	45.721	105.215	45.491	-4.1	Flutter	-0.50559

4.1 Validation

Linear aeroelastic analysis of the swept wing was carried out in order to verify the derived formulations. For this reason, experimental data for the flutter speed of the swept wing of Barmby *et al.* (1950) are used. The physical characteristics of the tested wings and their nondimensional parameters are presented in Table 1.

The linear flutter speed for each case is calculated and compared with those obtained by experiments for six different cases are given in Table 2. It can be seen that this formulation provides good agreement with the experimental data, and the difference between our proposed method and experimental data, in all six cases, is below 5%.

5. The First Order BH method(HB1)

The HB method is an efficient method for the prediction of the frequency and amplitude of LCO that occurs at speeds above the linear flutter speed for wings containing a cubic nonlinearity. In order to apply this method, plunge and pitch motions should assume the form of a trigonometric series, such as Fourier series. So, the time-dependent part of plunge and pitch motions can be approximated as

$$\begin{aligned}\xi(\tau) &= f_1 \sin(\omega\tau) + g_1 \cos(\omega\tau) \\ \alpha(\tau) &= a_1 \sin(\omega\tau)\end{aligned}\quad (17)$$

Substituting Eq. (17) into Eq. (6) and Eq. (8), and calculating the coefficients of $\sin(\omega\tau)$ and

$\cos(\omega\tau)$, we obtain the system a_1, f_1, g_1 and ω

$$\begin{aligned} m_1 a_1 + p_1 f_1 + q_1 g_1 + \frac{3}{4} A_5 \left(\frac{\bar{\omega}}{U^*}\right)^2 \beta_{\xi^3} f_1 (f_1^2 + g_1^2) &= 0 \\ m_2 a_1 + p_2 f_1 + q_2 g_1 + \frac{3}{4} A_5 \left(\frac{\bar{\omega}}{U^*}\right)^2 \beta_{\xi^3} g_1 (f_1^2 + g_1^2) &= 0 \\ m_3 a_1 + p_3 f_1 + q_3 g_1 + \frac{3}{4} A_6 \left(\frac{1}{U^*}\right)^2 \beta_{\alpha^3} a_1^3 &= 0 \\ m_4 a_1 + p_4 f_1 + q_4 g_1 &= 0 \end{aligned} \tag{18}$$

where m_i, p_i and q_i ($i=1, 2.. 4$) are functions of system parameters and frequency ω , and their definitions are given in Appendix C. For velocities larger than the bifurcation value, the motions have limited-amplitude, i.e., there exist non-zero solutions to Eq. (18).

At the particular case where we only have cubic nonlinearity in the pitch degree of freedom or $\beta_{\alpha^3} \neq 0$ and $\beta_{\xi^3} = 0$, the determinant of three equations of Eq. (18) should be zero. We can obtain acceptable frequency by the following equation

$$\begin{vmatrix} m_1 & m_2 & m_4 \\ p_1 & p_2 & p_4 \\ q_1 & q_2 & q_4 \end{vmatrix} = 0 \tag{19}$$

In this instance, once the frequency is obtained, f_1 and g_1 can be solved from the two relations of Eq. (18) in terms of a_1 , that is

$$\begin{aligned} f_1 &= -a_1(m_1 p_1 + m_2 p_2) / (p_1^2 + p_2^2) = a_1 F_1 \\ g_1 &= a_1(m_1 p_2 - m_2 p_1) / (p_1^2 + p_2^2) = a_1 G_1 \end{aligned} \tag{20}$$

Substituting Eq. (20) into the third equation of Eq. (18) pitch and plunge amplitude can be obtained:

Pitch amplitude/rad :

$$a_1 = 2U^* \sqrt{-\frac{(m_3 + p_3 F_1 + q_3 G_1)}{3A_6 \beta_{\alpha^3}}}$$

Plunge amplitude:

$$r_1 = \sqrt{f_1^2 + g_1^2} = a_1 \sqrt{F_1^2 + G_1^2} = 2U^* \sqrt{-\frac{(F_1^2 + G_1^2)(m_3 + p_3 F_1 + q_3 G_1)}{3A_6 \beta_{\alpha^3}}}$$

6. The third order BH method (HB3)

The second dominant harmonic is associated with a frequency of 3ω . For a higher order approximation in the analytical prediction, we rewrite Eq. (17) as

$$\begin{aligned} \xi(\tau) &= f_1 \sin(\omega\tau) + g_1 \cos(\omega\tau) + f_3 \sin(3\omega\tau) + g_3 \cos(3\omega\tau) \\ \alpha(\tau) &= a_1 \sin(\omega\tau) + a_3 \sin(3\omega\tau) + b_3 \cos(3\omega\tau) \end{aligned} \tag{21}$$

Substituting Eq.(17) into Eq.(6) and Eq.(8), and calculating the coefficients of $\sin(\omega\tau)$ and $\cos(\omega\tau)$, we obtain the system of $a_1, f_1, g_1, a_3, b_3, f_3, g_3$ and ω

$$\begin{aligned}
m_1 a_1 + p_1 f_1 + q_1 g_1 + \frac{3}{4} A_5 \left(\frac{\bar{\omega}}{U^*}\right)^2 \beta_{\xi^3} (-2g_1 g_3 f_1 + 2g_1^2 f_3 + f_1^3 + f_1 g_1^2 + 2f_1 f_3^2 + 2f_1 g_3^2 - f_1^2 f_3) &= 0 \\
m_2 a_1 + p_2 f_1 + q_2 g_1 + \frac{3}{4} A_5 \left(\frac{\bar{\omega}}{U^*}\right)^2 \beta_{\xi^3} (2g_1 f_3 f_1 + g_1^3 + f_1^2 g_1 - f_1^2 g_3 + 3g_1 f_3^2 + 2g_1 g_3^2 + 3g_1^2 g_3) &= 0 \\
m_3 a_1 + p_3 f_1 + q_3 g_1 + \frac{3}{4} A_6 \left(\frac{1}{U^*}\right)^2 \beta_{\alpha^3} (-a_1^2 a_3 + a_1^3 + 2a_1 a_3^2 + 2a_1 b_3^2) &= 0 \\
m_4 a_1 + p_4 f_1 + q_4 g_1 - \frac{3}{4} A_6 \left(\frac{1}{U^*}\right)^2 \beta_{\alpha^3} a_1^2 b_3 &= 0 \\
m_{13} a_3 + v_{13} b_3 + p_{13} f_3 + q_{13} g_3 + \frac{3}{4} A_5 \left(\frac{\bar{\omega}}{U^*}\right)^2 \beta_{\xi^3} (-f_1^3 / 3 + 2f_3^3 + f_3 g_3^2 + 2f_1^2 f_3 + f_1 g_1^2 + 2g_1^2 f_3) &= 0 \\
m_{23} a_3 + v_{23} b_3 + p_{23} f_3 + q_{23} g_3 + \frac{3}{4} A_5 \left(\frac{\bar{\omega}}{U^*}\right)^2 \beta_{\xi^3} (2f_1^2 g_3 + 12g_1^2 g_3 - 2f_1^2 g_1 + g_1^3 / 3 + f_3^2 g_3 + g_3^3) &= 0 \\
m_{33} a_3 + v_{33} b_3 + p_{33} f_3 + q_{33} g_3 + \frac{3}{4} A_6 \left(\frac{1}{U^*}\right)^2 \beta_{\alpha^3} (a_3 b_3^2 + 2a_1^2 a_3 - a_1^3 / 3 + a_3^3) &= 0 \\
m_{43} a_3 + v_{43} b_3 + p_{43} f_3 + q_{43} g_3 + \frac{3}{4} A_6 \left(\frac{1}{U^*}\right)^2 \beta_{\alpha^3} (a_3^2 b_3 + 2a_1^2 b_3 + b_3^3) &= 0
\end{aligned} \tag{22}$$

where $m_i, m_{i3}, p_i, p_{i3}, v_{i3}, q_i, q_{i3}$ ($i=1, 2, \dots, 4$) are functions of system parameters and frequency ω , and their expressions are given in Appendix C. Also variables m_i, p_i and q_i ($i=1, 2, \dots, 6$) are the same as mentioned in HB1 method.

Again At the particular case where we only have cubic nonlinearity in the pitch degree of freedom or $\beta_{\alpha^3} \neq 0$ and $\beta_{\xi^3} = 0$, the variables f_1, g_1 in terms of a_1 can be solved from the two expressions in Eq. (22), and their solutions are the same as Eq. (20). Also the variables f_3, g_3 can be solved from other two expressions in Eq. (22) in terms of a_3 and b_3

$$\begin{aligned}
f_3 &= -a_3(m_{13}p_{13} + m_{23}p_{23}) / (p_{13}^2 + p_{23}^2) - b_3(m_{13}p_{23} - m_{23}p_{13}) / (p_{13}^2 + p_{23}^2) = F_{3a}a_3 + F_{3b}b_3 \\
g_3 &= a_3(m_{13}p_{23} - m_{23}p_{13}) / (p_{13}^2 + p_{23}^2) - b_3(m_{13}p_{13} - m_{23}p_{23}) / (p_{13}^2 + p_{23}^2) = G_{3a}a_3 + G_{3b}b_3
\end{aligned} \tag{23}$$

So the other four expressions of Eq. (22) are

$$\begin{aligned}
M_3 a_1 + \frac{3}{4} A_6 \left(\frac{1}{U^*}\right)^2 \beta_{\alpha^3} (-a_1^2 a_3 + a_1^3 + 2a_1 a_3^2 + 2a_1 b_3^2) &= 0 \\
M_4 a_1 - \frac{3}{4} A_6 \left(\frac{1}{U^*}\right)^2 \beta_{\alpha^3} a_1^2 b_3 &= 0 \\
M_{33} a_3 + N_{33} b_3 + \frac{3}{4} A_6 \left(\frac{1}{U^*}\right)^2 \beta_{\alpha^3} \left(a_3 b_3^2 + 2a_1^2 a_3 - \frac{a_1^3}{3} + a_3^3\right) &= 0 \\
M_{43} a_3 + N_{43} b_3 + \frac{3}{4} A_6 \left(\frac{1}{U^*}\right)^2 \beta_{\alpha^3} (a_3^2 b_3 + 2a_1^2 b_3 + b_3^3) &= 0
\end{aligned} \tag{24}$$

Where

$$\begin{aligned}
M_3 &= m_3 + p_3 F_1 + q_3 G_1 \\
M_4 &= m_4 + p_4 F_1 + q_4 G_1 \\
M_{33} &= m_{33} + p_{33} F_{3a} + q_{33} G_{3a} \\
N_{33} &= v_{33} + p_{33} F_{3b} + q_{33} G_{3b}
\end{aligned}$$

$$\begin{aligned} M_{43} &= -N_{33} = m_{43} + p_{43}F_{3a} + q_{43}G_{3a} \\ N_{43} &= M_{33} = v_{43} + p_{43}F_{3b} + q_{43}G_{3b} \end{aligned} \tag{25}$$

Lee *et al.* (2005), solved a equation similar to Eq. (24) for a 2-DOF airfoil after some complicated algebraic manipulations. Taking advantage of the suggested relations, we have:

$$M_4^5 - 8M_4^4M_{43} + M_4^3(10M_{43}^2 + 4M_{33}^2 + M_3^2 - 4M_{33}M_3) + M_4^2(30M_{43}M_{33}M_3 - 9M_{43}M_{33}^2 - 12M_{43}M_3^2 - 24M_{43}^2) + M_4(36M_{43}^2M_3^2 - 30M_{43}^2M_{33}M_3 + 9M_{43}^4 + 9M_{43}^2M_{33}^2) + 3M_{43}^3M_3^2 = 0$$

$$\begin{aligned} a_1^2 &= \frac{U^{*2}}{\beta_{\alpha^3}} \cdot \frac{4M_{43}(M_3M_{43} + M_4M_{33})}{M_4^2 - 4M_3M_{43} - 3M_{43}^2} \\ a_3^2 + b_3^2 &= \frac{U^{*2}}{A_6\beta_{\alpha^3}} \cdot \frac{4M_{43}(M_3M_4 + M_4M_{33})}{3(M_4^2 - 4M_3M_{43} - 3M_{43}^2)} \end{aligned} \tag{26}$$

By using Eq. (25), we can obtain acceptable frequency, and then by substituting Eq. (26) into the two expressions of Eq. (24), a_1, a_3 and b_3 could be found. Consequently, from Eq. (20) and Eq. (21), we can derive the specific values of f_1, g_1 and f_3, g_3 , respectively.

7. Determining turning point location

Turning point exists only in subcritical bifurcations where the amplitudes of the unstable and stable LCO become equal to each other as well as frequency. In a swept wing with cubic nonlinearity, the characteristics of the wing and the sign of pitch cubic nonlinearity, affect the TP location, irrespective of its magnitude and initial conditions.

In this section by utilizing HB1 method, we investigate how the characteristics of the wing affect the location of TP and how the subcritical bifurcation converts to supercritical one or vice versa. The results are consistent with when the HB3 method is applied. A typical application of Runge-Kutta algorithm fails to estimate this location because typically there is no proper initial disturbance for finding this location. The wing parameters are as follow:

$$\mu = 100, x_a = 0.25, a_h = -0.3, r_a = 0.5, l/b_n = 50, \bar{\omega} = 1.2, \beta_a = 1, \beta_{\alpha^3} = 40, \beta_{\xi} = 1, \beta_{\xi^3} = 0, \Lambda = 30^\circ$$

The location of turning point of the wing with respect to the variation of wing parameters is depicted in Fig. 2.

By increasing a_h supercritical bifurcation converts to the subcritical at $a_h = -0.47$ and it causes the TP location gets more far away from the Hopf point. Moreover, by increasing r_a supercritical bifurcation converts to the subcritical at $r_a = 0.32$. This phenomenon is repeated again for $\bar{\omega}$ and the conversion from supercritical to subcritical bifurcation occurs in $\bar{\omega} = 1.04$.

8. Bifurcation plots

Supercritical bifurcation emerges, when a wing with the characteristics mentioned in Sec. 7, including cubic hardening stiffness in the pitch degree of freedom, is considered.

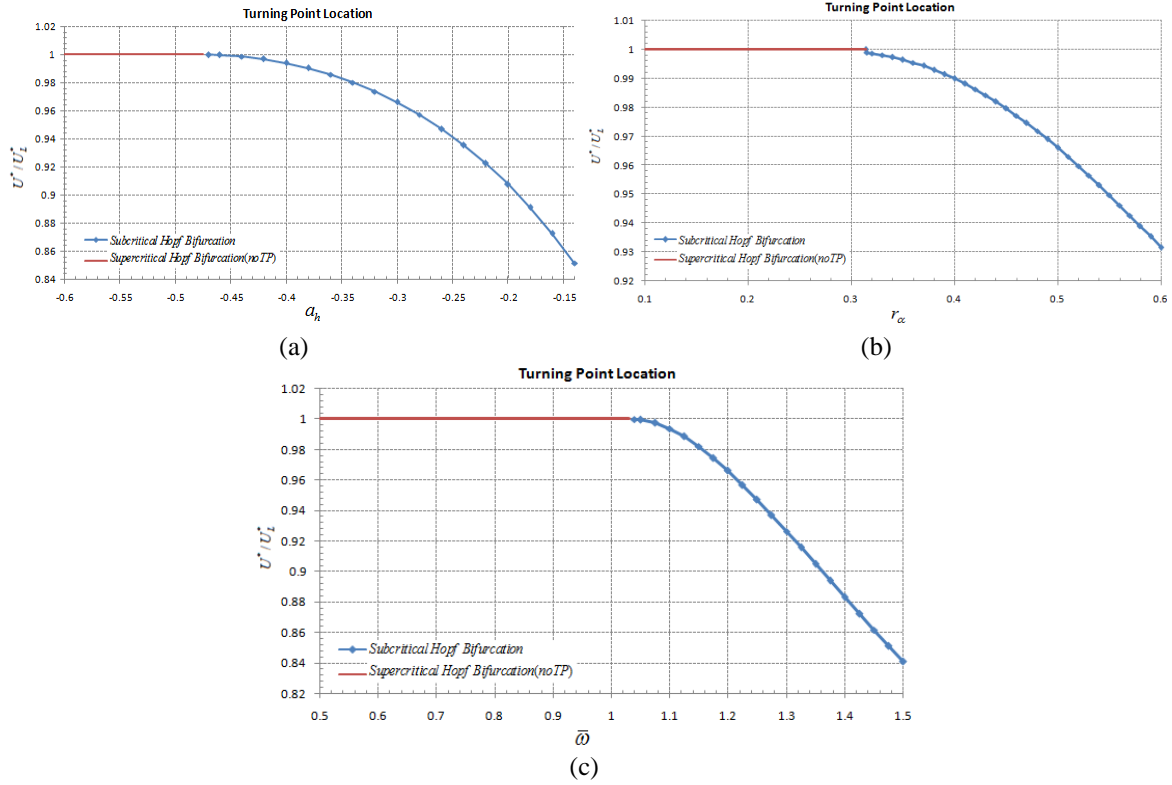


Fig. 2 TP location with respect to the variation of (a) a_h (b) r_α (c) $\bar{\omega}$

To check the validation of results, stable LCO's at various U^*/U_L^* are numerically evaluated and compared with those obtained by Ghadiri *et al.* (2007) and reported in Table 3, and good agreement is observed. Here the wing has no sweep angle and the results are for the mid section of the wing.

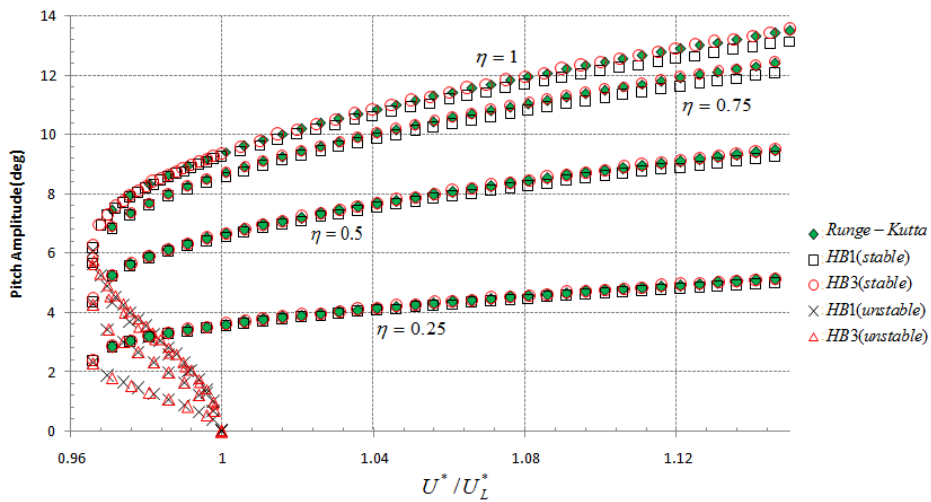
The pitch and plunge amplitudes obtained via different methods (i.e., Runge-Kutta, HB1, HB3) are compared with each other in Tables 3 and 4. It can be realized that, in stable LCO condition, all methods have same results with small difference.

Table 3 Validation of wing pitch amplitude.

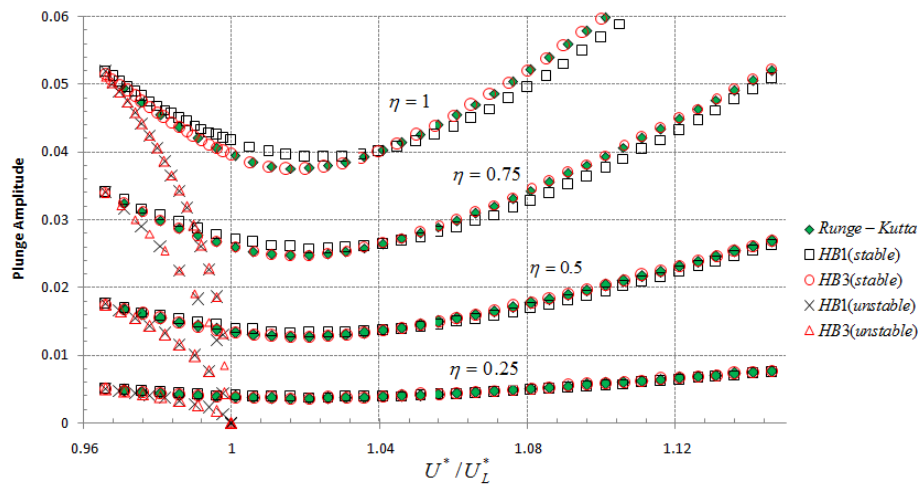
U^*/U_L^*	HB1 present	HB1 Ghadiri <i>et al.</i> (2007)	HB3 present	HB3 Ghadiri <i>et al.</i> (2007)	Runge-kutta present	Runge-kutta Ghadiri <i>et al.</i> (2007)
1.005	2.522169	2.522232	2.524398	2.524287	2.524225	2.524312
1.045	7.637217	7.637241	7.696709	7.689807	7.691579	7.691588
1.075	9.927706	9.927723	10.05102	10.036279	10.042526	10.042542
1.1	11.528767	11.528789	11.71012	11.690238	11.702814	11.702847
1.135	13.500821	13.500811	13.76358	13.742102	13.767989	13.767986
1.15	14.278625	14.278636	14.57505	14.555414	14.588522	14.588624

Table 4 Validation of wing plunge amplitude.

U^*/U_L^*	HB1 present	HB1 Ghadiri <i>et al.</i> (2007)	HB3 present	HB3 Ghadiri <i>et al.</i> (2007)	Runge-kutta present	Runge-kutta Ghadiri <i>et al.</i> (2007)
1.005	0.079809	0.079811	0.079729	0.79739	0.079734	0.079736
1.045	0.244428	0.244429	0.242566	0.242694	0.242689	0.24269
1.075	0.320237	0.320237	0.316775	0.316968	0.31695	0.31695
1.1	0.374169	0.374169	0.369543	0.369717	0.369682	0.369681
1.135	0.441699	0.441698	0.435901	0.435953	0.435889	0.435889
1.15	0.468665	0.468665	0.462549	0.46254	0.462465	0.462466

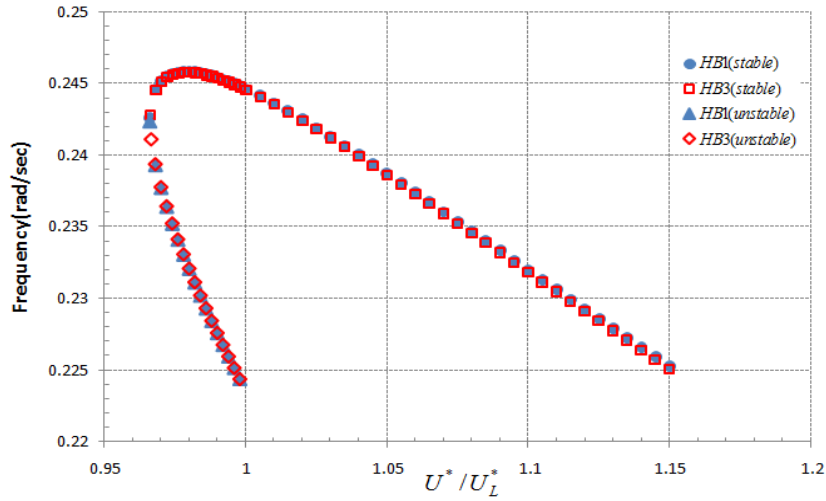


(a)



(b)

Fig. 3 finite limited amplitude of the stable and unstable LCOs for different wing sections (a) pitch amplitude (b) plunge amplitude (c) frequency



(c)
Fig. 3 Continued

Now, by using the HB1 and HB3 methods, the finite limited pitch and plunge amplitudes of the stable and unstable LCOs as well as LCO frequency, for the swept wing are computed and compared with numerical Runge-Kutta method in Fig. 3 for different span-wise positions.

It is concluded from this plot that for greater values of U^*/U_L^* there are some difference between different solution methods. Also the differences between three methods are increased for greater values of η . Here the turning point location is near $U^*/U_L^* = 0.967$. Another interesting result is that for all sections of the wing, the TP location is same. Moreover, the LCO frequency first increases until turning point and then decreases.

Among the different investigations, the effects of different parameters on Subcritical and Supercritical knee-like Hopf bifurcation diagrams, for wing tip, are studied and plotted in Fig. 4.

In this figure, the bifurcation diagrams for different values of a_h and μ are plotted. It is seen that for $a_h = -0.6$ the Supercritical knee-like Hopf bifurcation condition is obtained, but in $a_h = -0.3$

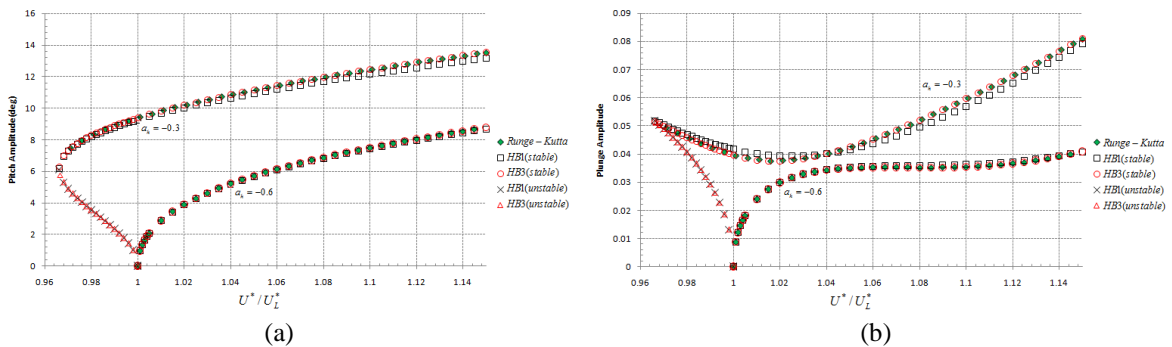
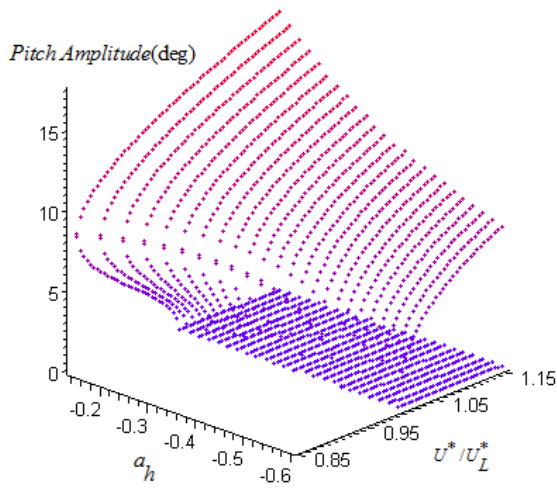
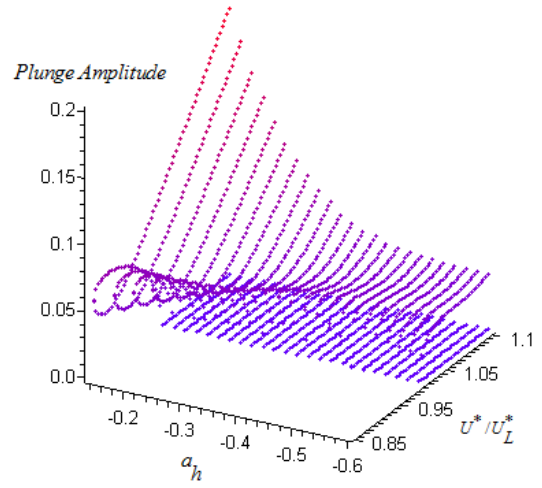


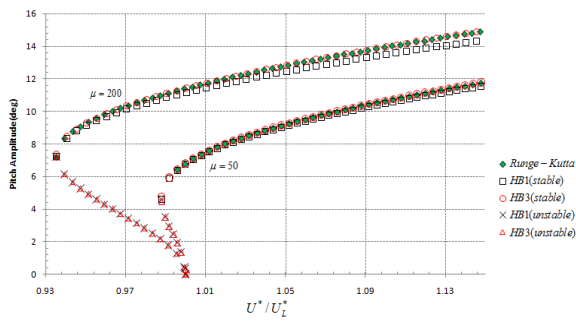
Fig. 4 Subcritical and Supercritical knee-like Hopf bifurcation diagram against different parameters (a), (b), (c), (d) pitch and plunge amplitude vs. different value of a_h (c), (d) pitch and plunge amplitude vs. different value of μ



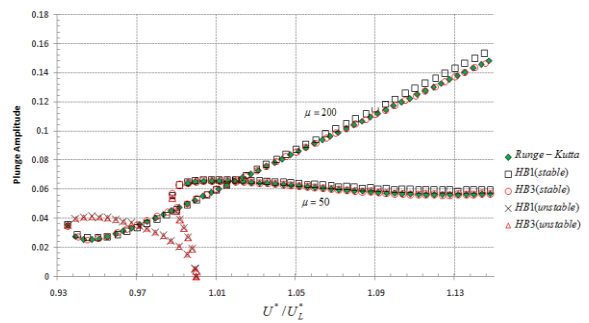
(c)



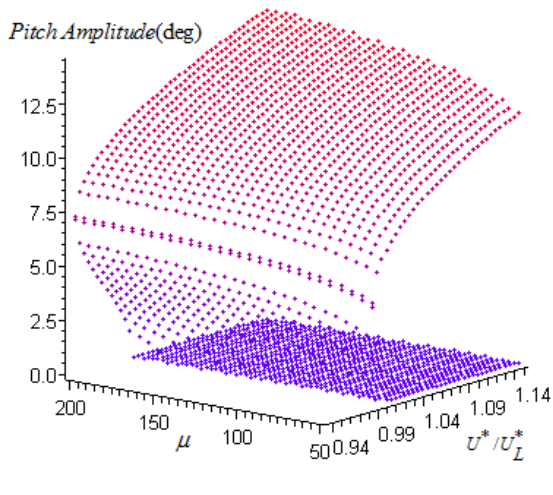
(d)



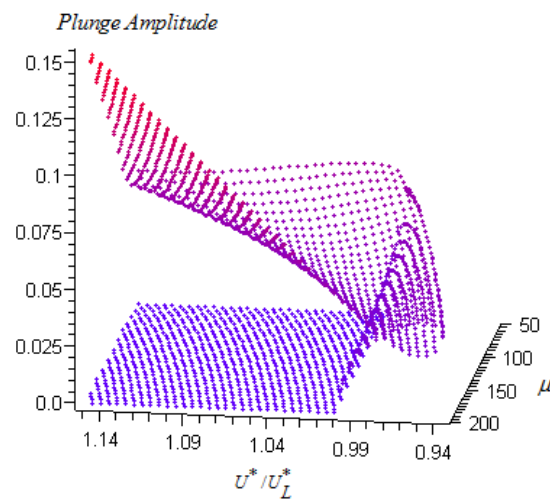
(e)



(f)



(g)



(h)

Fig. 4 Continued

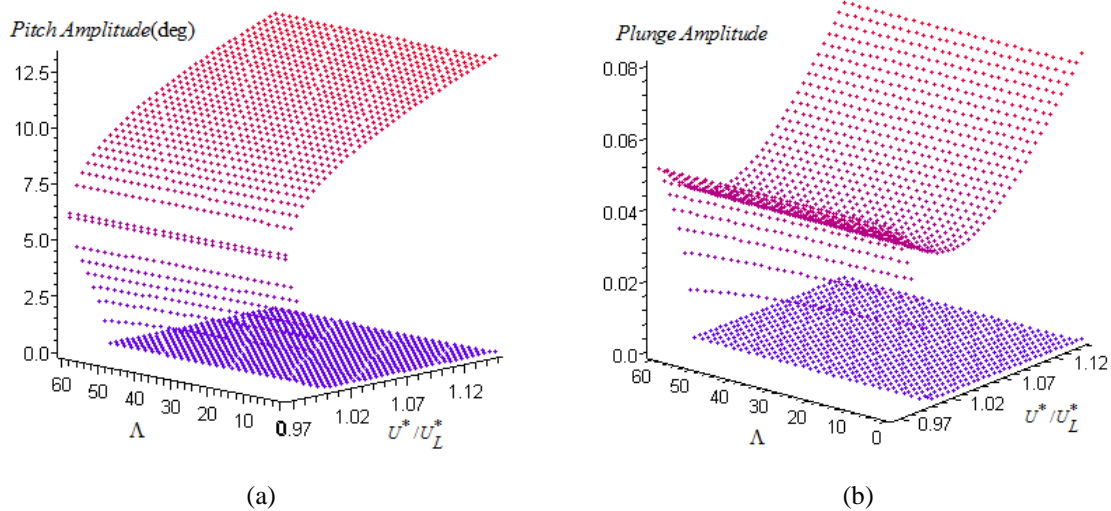


Fig. 5 Subcritical and Supercritical knee-like Hopf bifurcation diagram against wing sweep angle (a), (b) pitch and plunge amplitude

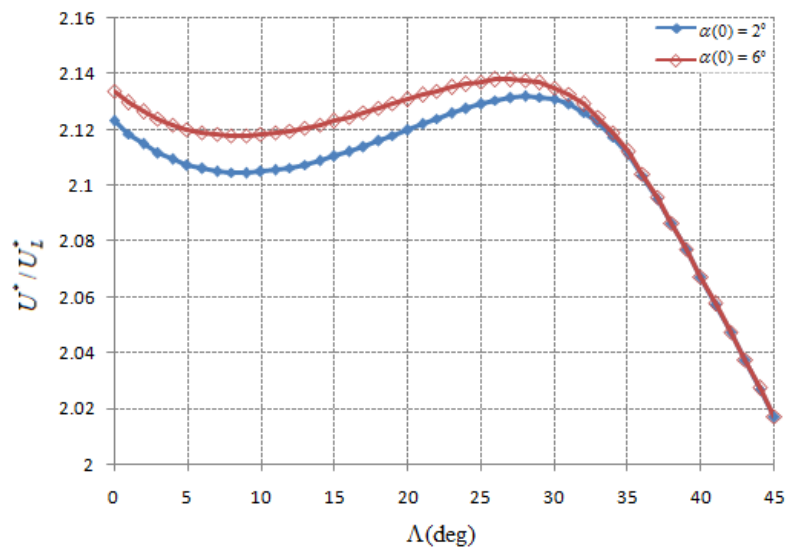


Fig. 6 Bifurcation onset location against wing sweep angle for two different initial conditions

the system examines the Subcritical condition. Moreover, for different system parameters, different turning point locations are obtained. Also when μ increases, the turning point appears in lower values of speed.

In Fig. 5 Subcritical and Supercritical knee-like Hopf bifurcation diagram against different values of sweep angle are plotted.

As it can be seen, the variation of sweep angle has not had significant effects on amplitudes.

In Fig. 6 the effect of wing sweep angle on bifurcation location of a wing with following characteristics for two different initial pitch conditions, is plotted.

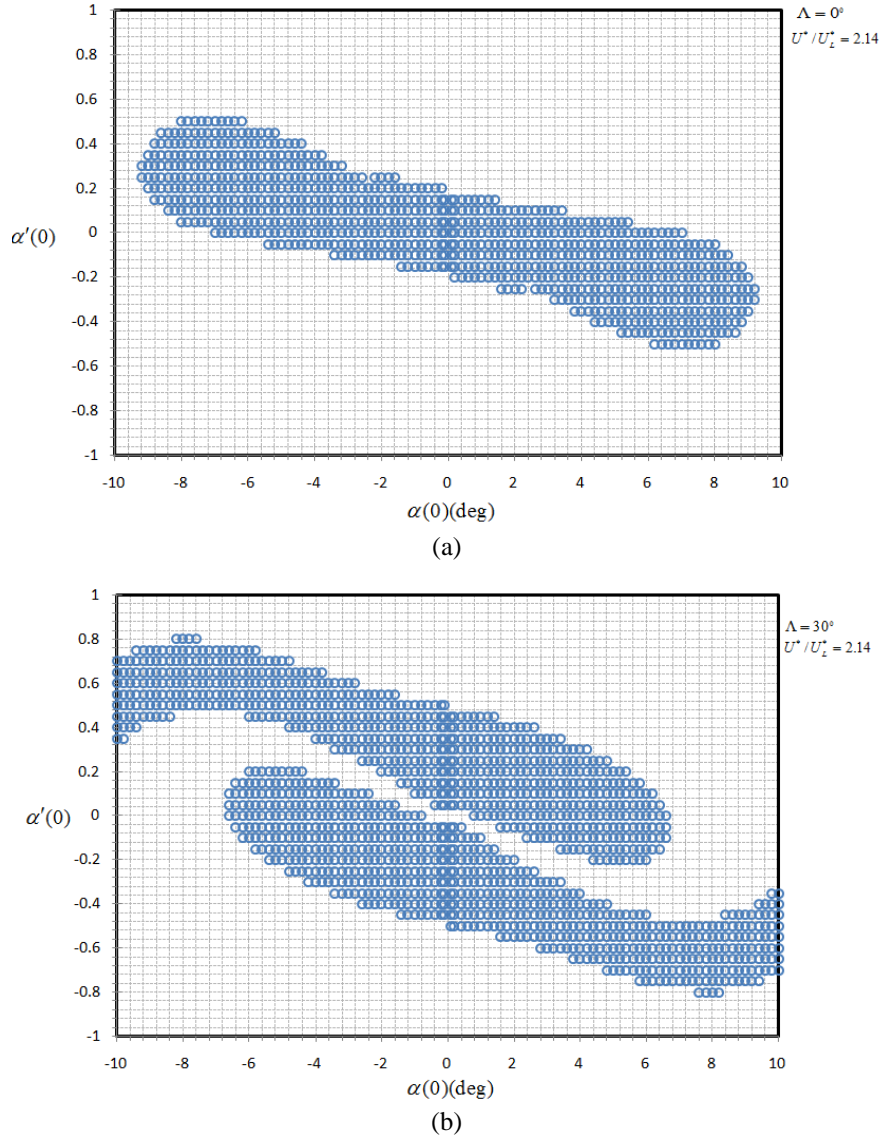


Fig. 7 Bifurcation locations for different values of $\alpha(0)$ and $\alpha'(0)$ for (a) $\Lambda=0^\circ$ (b) $\Lambda=30^\circ$

$$\mu = 100, x_a = 0.25, a_h = -0.5, r_a = 0.5, l/b_n = 50, \bar{\omega} = 0.2, \beta_a = 1, \beta_{a_3} = 80, \beta_\xi = 1, \beta_{\xi_3} = 0, \Lambda = 30^\circ,$$

$$\xi(0) = \xi'(0) = \alpha'(0) = 0, \alpha(0) = 2^\circ, \eta = 1.$$

As it can be seen in this figure, for zero sweep angles in the first case, the bifurcation is occurred in $U^*/U_L^*=2.14$ but this value decreases until $\Lambda=9^\circ$. After this point, the bifurcation nondimensional speed increases until $\Lambda=27^\circ$ and for sweep angles greater than this value, the bifurcation speed again decreases. The trend of the second case shown in this figure is same as the first one, but the values are different. It is concluded from this plot that for sweep angles lower

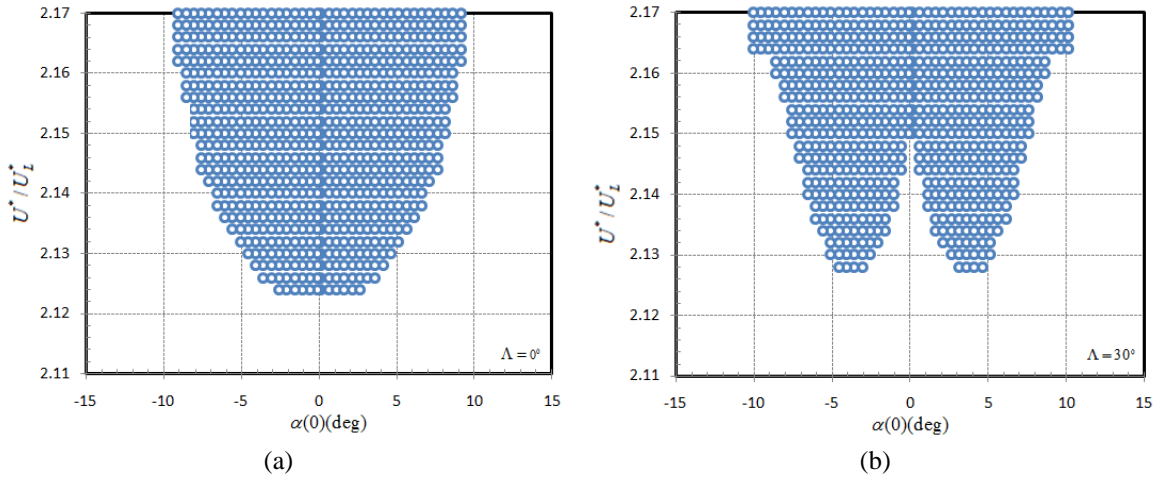


Fig. 8 Bifurcation locations for different values of $\alpha(0)$ and U^*/U_L^* for (a) $\Lambda=0$ (b) $\Lambda=30^\circ$

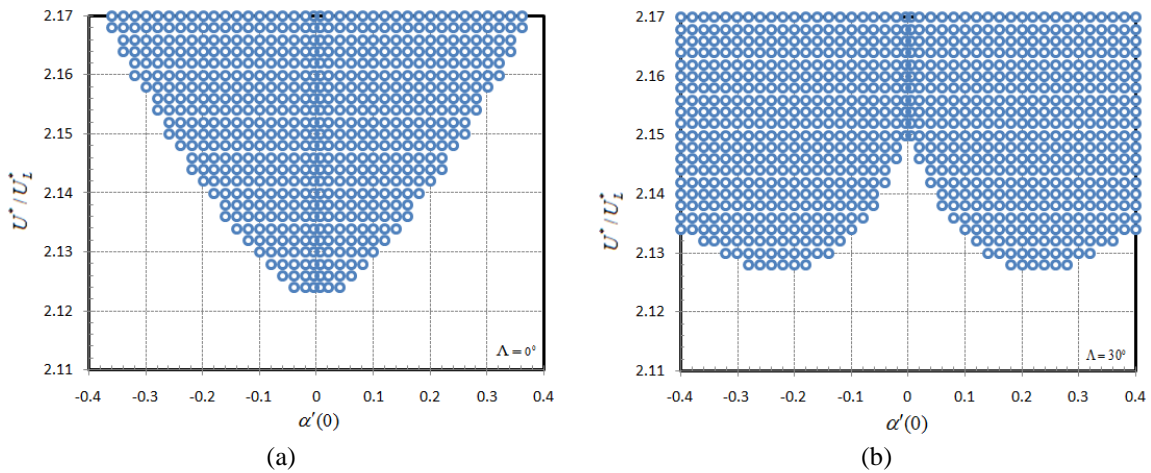


Fig. 9 Bifurcation locations for different values of $\alpha'(0)$ and U^*/U_L^* for (a) $\Lambda=0$ (b) $\Lambda=30^\circ$

than or equal of 33 degree, the variation of initial condition has significant effects on the location of bifurcation onset. But in greater values of sweep angle, the location of bifurcation is independent of the initial conditions.

In Figs. 7 to 11, the bifurcation locations of the prescribed wing with and without sweep angle for different value of initial condition for two different nondimensional speed are plotted. The region that bifurcation occurred is obviously different between the wing with sweep and without it, in all figures. In Fig. 7, it is seen that bifurcation region for swept wing is bigger than the unswept wing.

As it is clear from this plot, the bifurcation location is divided into two parts and between these two parts there are some initial conditions in which the wing doesn't examine the bifurcation phenomenon. In Fig. 8, the bifurcation location is plotted for different values of U^*/U_L^* and $\alpha(0)$. Here, the region that bifurcation occurred for wing with sweep angle is smaller than the unswept.

In Fig. 9 the bifurcation location is plotted against different value of U^*/U_L^* and $\alpha'(0)$. The

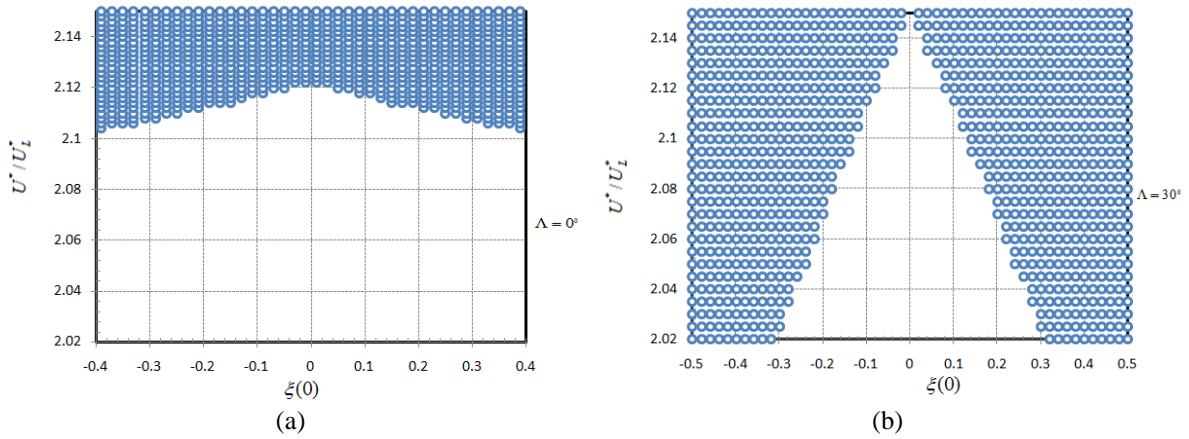


Fig. 10 Bifurcation locations for different values of $\zeta(0)$ and U^*/U_L^* for (a) $\Lambda=0$ (b) $\Lambda=30^\circ$

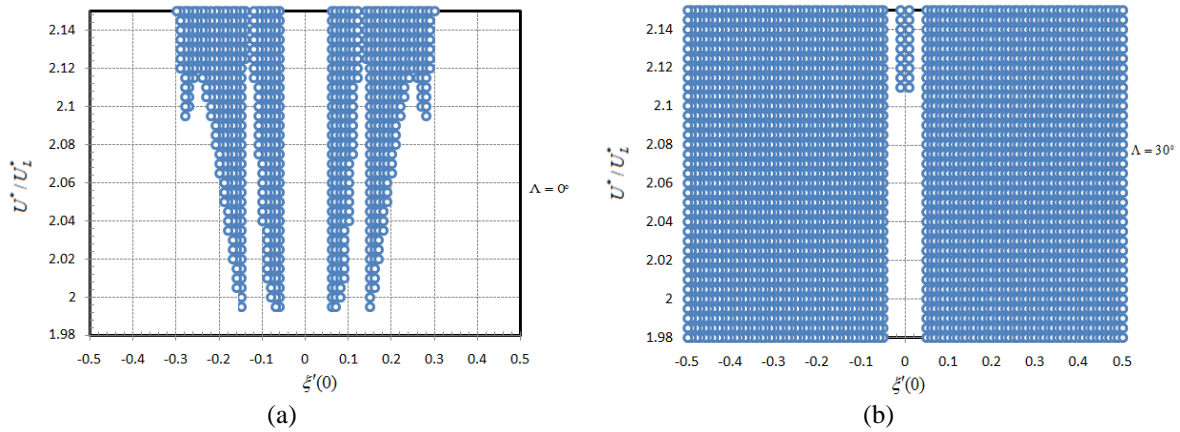


Fig. 11 Bifurcation locations for different values of $\zeta'(0)$ and U^*/U_L^* for (a) $\Lambda=0$ (b) $\Lambda=30^\circ$

bifurcation region for swept wing is bigger than the unswept wing except for somewhere near $\alpha'(0)=0$.

Furthermore, the bifurcation location for $\zeta(0)$ and $\zeta'(0)$ are plotted in Figs. 10 and 11. In both plots the bifurcation region for swept wing is bigger than unswept wing.

In Fig. 11 the bifurcation location is so big that we can say in all initial conditions the bifurcation phenomenon is occurred.

9. Conclusions

In this work, the governing aeroelastic equations of a swept wing in an incompressible flow were derived in the time domain. The nonlinear aeroelastic behavior of the wing with hardening cubic nonlinearities in the pitch degree of freedom was studied. Moreover, the prediction of LCO amplitude was investigated by using the HB method and numerical solution and the results were illustrated in bifurcation plots. The different Supercritical and Subcritical knee-like Hopf

bifurcation diagrams, for different system parameters, were plotted and the following outcomes were concluded:

- (a) The bifurcation diagram is highly dependent on the position of the elastic center.
- (b) The type of bifurcation and TP location depend on the characteristics of the wing as well as the structural nonlinearity parameters.
- (c) The type of bifurcation is strictly depends on the value of structural nonlinearity parameter.
- (d) The wing sweep angle has significant effect on the location of bifurcation.
- (e) For the high values of sweep angle, the location of bifurcation is independent of the initial conditions.

References

- Anton, C., Deng J. and Wong, Y.S. (2012), "Hopf bifurcation analysis of an aeroelastic model using stochastic normal form", *J. Sound Vib.*, **331**, 3866-3886.
- Barmby, J.C., Cunningham, H.J. and Garrick, I.E. (1950), *Study of effects of sweep on the flutter of cantilever wings*, NACA TN 2121.
- Bisplinghoff, R.L., Ashley, H. and Halfman, R.L. (1955), *Aeroelasticity*, Addison-Wesley Publication Co., Reading, MA, USA.
- Breitbart, E.J. (1977), "Effect of structural nonlinearities on aircraft vibration and flutter", *Proceedings of the 45th Structures and Materials AGARD Panel Meeting*, AGARD Report 665, Voss, Norway.
- Conner, M.D., Tang, D.M., Dowell, E.H. and Virgin, L.N. (1997), "Nonlinear behavior of a typical airfoil section with a control surface freeplay: a numerical and experimental study", *J. Fluid. Struct.*, **11**, 89-109.
- Dessi, D. and Mastroddi, F. (2004), "Limit-cycle stability reversal via singular perturbation and wing-flap flutter", *J. Fluid. Struct.*, **19**, 765-783.
- Dessi, D., Mastroddi, F. and Morino, L. (2002), "Limit-cycle stability reversal near a hopf bifurcation with aeroelastic applications", *J. Sound Vib.*, **256**, 347-365.
- Dowell, E.H., Crawley, H.C., Curtiss, H.C., Peters, D.A., Scanlan, R.H. and Sisto, F. (1995), *A Modern course in Aeroelasticity*, Kluwer Academic Publisher.
- Eken, S. and Kaya, M.O. (2015), "The effect of sweep angle on the limit cycle oscillation of aircraft wings", *Adv. Aircraft Spacecraft Sci.*, **2**, 199-215.
- Ghadiri, B. and Razi, M. (2007), "Limit cycle oscillations of rectangular cantilever wings containing cubic nonlinearity in an incompressible flow", *J. Fluid. Struct.*, **23**, 665-680.
- Haddapour, H., Kouchakzadeh, M.A. and Shadmehri, F. (2008), "Aeroelastic Instability of aircraft composite wings in an incompressible flow", *J. Compos. Struct.*, **83**, 93-99.
- Irani, S., Sarrafzadeh, H. and Amoozgar, M.R. (2011), "Bifurcation in a 3-DOF Airfoil with Cubic Structural Nonlinearity", *Chin. J. Aeronaut.*, **24**, 265-278.
- Jones, R.T. (1940), *The unsteady lift of a wing of finite aspect ratio*, NACA Report 681.
- Kim, S.H. and Lee, I. (1996), "Aeroelastic analysis of a flexible airfoil with a freeplay nonlinearity", *J. Sound Vib.*, **193**, 923-846.
- Laurenson, R.M. (1980), "Flutter analysis of missile control surface containing structural nonlinearities", *AIAA J.*, **18**, 1245-1251.
- Lee, B.H.K. and Tron, A. (1989), "Effects of structural nonlinearities on flutter characteristics of the CF-18 aircraft", *J. Aircraft*, **26**, 781-786.
- Lee, B.H.K., Gong, L. and Wong, Y. (1997), "Analysis and computation of nonlinear dynamic response of a two-degree-of-freedom system and its application in Aeroelasticity", *J. Fluid. Struct.*, **11**, 225-246.
- Lee, B.H.K., Liub, L. and Chung, K.W. (2005), "Airfoil motion in subsonic flow with strong cubic nonlinear restoring forces", *J. Sound Vib.*, **28**, 699-717.
- O'Neil, T. and Strganac, T.W. (1998), "Aeroelastic response of a rigid wing supported by nonlinear

- springs”, *J. Aircraft*, **35**, 616-622.
- Peng, C. and Han, J. (2011), “Numerical investigation of the effects of structural geometric and material nonlinearities on limit-cycle oscillation of a cropped delta wing”, *J. Fluid. Struct.*, **27**, 611-622.
- Sedaghat, A., Cooper, J.E., Leung, A.Y.T. and Wright, J.R. (2001), “Estimation of the hopf bifurcation point for aeroelastic systems”, *J. Sound Vib.*, **248**, 31-42.
- Shen, S.F. (1977), “An approximate analysis of nonlinear flutter problems”, *J. Aerosp. Sci.*, **26**, 25-32.
- Sheta, E.F., Harrand, V.J., Thompson, D.E. and Strganac, T.W. (2002), “Computational and experimental investigation of limit cycle oscillations of nonlinear aeroelastic systems”, *J. Aircraft*, **39**, 133-141.
- Tang, D., Dowell, E.H. and Virgin, L.N. (1998), “Limit cycle behavior of an airfoil with a control surface”, *J. Fluid. Struct.*, **12**, 839-858.
- Tang, D.M. and Dowell, E.H. (1992), “Flutter and Stall Response of a Helicopter Blade with Structural Nonlinearity”, *J. Aircraft*, **29**, 953-960.
- Theodorsen, T. (1935), *General theory of aerodynamic instability and the mechanism of flutter*, NACA Report 496.
- Woolston, D.S., Runyan, H.L. and Andrews, R.E. (1957), “An investigation of effects of certain types of structural nonlinearities on wing and control surface flutter”, *J. Aeronaut. Sci.*, **24**, 57-63.

CC

Nomenclature

a_h	non dimensional distance from wing mid-chord to elastic axis
b	wing semi-chord
h	plunge displacement
HB1, HB2	first and third order harmonic balance method
I_α	wing mass moment of inertia about elastic axis
L	wing aerodynamic lift force
LCO	Limit cycle oscillations
m	wing mass per unit length
M_α	wing pitching moment about elastic
$M_\alpha(\alpha)$	nonlinear pitch stiffness terms
t	time(s)
TP	turning point
U_L^*	Linear flutter speed
U_n	free-stream velocity normal to swept wing
U_n^*	non-dimensional velocity normal to swept wing
x_α	non-dimensional distance from the wing elastic axis to the centre of mass
α	pitch angle of wing
$\beta_\alpha, \beta_{\alpha^3}$	constants in nonlinear term $M_\alpha(\alpha)$
β_ξ, β_{ξ^3}	constants in nonlinear term $G(\xi)$
$\varepsilon_1, \varepsilon_2$	constants in Wagner’s function
ζ_ξ, ζ_α	viscous damping ratio in plunge and pitch
μ	wing-air mass ratio
ρ	density of air
ζ	non dimensional plunge displacement

τ	non dimensional time
ψ_1, ψ_2	constants in Wagner's function
ω	fundamental frequency of the motion
$\omega_\xi, \omega_\alpha$	natural frequencies in plunge and
$G(\xi)$	nonlinear plunge stiffness terms
Λ	Wing sweep angle

Appendix A

The coefficients of the Eqs. (2) and (8) are as follow

$$\begin{aligned}
 A_1 &= \int_0^l (F_h(\eta)) d\eta & A_2 &= \int_0^l (F_\alpha(\eta)) d\eta & A_3 &= \int_0^l \left(\frac{d^2 F_h(\eta)}{d\eta^2} \right)^2 d\eta & A_4 &= \int_0^l \left(\frac{dF_\alpha(\eta)}{d\eta} \right)^2 d\eta \\
 A_5 &= \int_0^l (F_h(\eta))^2 d\eta & A_6 &= \int_0^l (F_\alpha(\eta))^2 d\eta & A_7 &= \int_0^l (F_h(\eta) F_\alpha(\eta)) d\eta & A_8 &= \int_0^l \left(F_h(\eta) \frac{dF_h(\eta)}{d\eta} \right) d\eta \\
 A_9 &= \int_0^l \left(F_h(\eta) \frac{dF_\alpha(\eta)}{d\eta} \right) d\eta & A_{10} &= \int_0^l \left(F_\alpha(\eta) \frac{dF_h(\eta)}{d\eta} \right) d\eta & A_{11} &= \int_0^l \left(F_\alpha(\eta) \frac{dF_\alpha(\eta)}{d\eta} \right) d\eta & A_{12} &= \int_0^l \left(F_h(\eta) \frac{d^2 F_h(\eta)}{d\eta^2} \right) d\eta \\
 A_{13} &= \int_0^l \left(F_h(\eta) \frac{d^2 F_\alpha(\eta)}{d\eta^2} \right) d\eta & A_{14} &= \int_0^l \left(F_\alpha(\eta) \frac{d^2 F_h(\eta)}{d\eta^2} \right) d\eta & A_{15} &= \int_0^l \left(F_\alpha(\eta) \frac{d^2 F_\alpha(\eta)}{d\eta^2} \right) d\eta \\
 c_a &= A_5 + \frac{A_5}{\mu} & c_b &= A_7 x_a - \frac{a_h A_7}{\mu} & c_1 &= \frac{1}{\mu} \left[2A_5(\psi_1 \varepsilon_1 + \psi_2 \varepsilon_2) + \frac{2b_n \tan \Lambda}{l} A_8(1 - \psi_1 - \psi_2) + \left(\frac{b_n \tan \Lambda}{l} \right)^2 A_{12} \right] \\
 c_2 &= 2A_5 \zeta_{\bar{\omega}} \left(\frac{\bar{\omega}}{U_n^*} \right) + \frac{2}{\mu} \left[A_5(1 - \psi_1 - \psi_2) + \frac{b_n \tan \Lambda}{l} A_8 \right] \\
 c_3 &= \frac{1}{\mu} \left[2A_7(1 - \psi_1 - \psi_2) + 2 \left(\frac{1}{2} - a_h \right) \left(A_7(\psi_1 \varepsilon_1 + \psi_2 \varepsilon_2) + \frac{b_n \tan \Lambda}{l} A_9(1 - \psi_1 - \psi_2) \right) + \frac{b_n \tan \Lambda}{l} A_9 - a_h \left(\frac{b_n \tan \Lambda}{l} \right)^2 A_{13} \right] \\
 c_4 &= \frac{1}{\mu} \left[2 \left(\frac{1}{2} - a_h \right) A_7(1 - \psi_1 - \psi_2) - a_h \frac{2b_n \tan \Lambda}{l} A_9 + A_7 \right] \\
 c_5 &= \frac{2}{\mu} \left[-\psi_1 \varepsilon_1^2 A_5 + \frac{b_n \tan \Lambda}{l} \psi_1 \varepsilon_1 A_8 \right] & c_6 &= \frac{2}{\mu} \left[-\psi_2 \varepsilon_2^2 A_5 + \frac{b_n \tan \Lambda}{l} \psi_2 \varepsilon_2 A_8 \right] \\
 c_7 &= \frac{2}{\mu} \left[\psi_1 \varepsilon_1 A_7 \left(1 - \left(\frac{1}{2} - a_h \right) \varepsilon_1 \right) + \frac{b_n \tan \Lambda}{l} \psi_1 \varepsilon_1 \left(\frac{1}{2} - a_h \right) A_9 \right] \\
 c_8 &= \frac{2}{\mu} \left[\psi_2 \varepsilon_2 A_7 \left(1 - \left(\frac{1}{2} - a_h \right) \varepsilon_2 \right) + \frac{b_n \tan \Lambda}{l} \psi_2 \varepsilon_2 \left(\frac{1}{2} - a_h \right) A_9 \right] \\
 d_a &= A_7 \left(\frac{x_a}{r_a^2} \right) - \frac{a_h A_7}{\mu r_a^2} & d_b &= A_6 + \frac{1}{\mu} \left(\frac{1}{8} + a_h^2 \right) A_6 \\
 d_1 &= -\frac{1}{\mu r_a^2} \left[(1 + 2a_h) A_7(\psi_1 \varepsilon_1 + \psi_2 \varepsilon_2) + \frac{b_n \tan \Lambda}{l} (1 + 2a_h) A_{10}(1 - \psi_1 - \psi_2) + a_h \left(\frac{b_n \tan \Lambda}{l} \right)^2 A_{14} \right] \\
 d_2 &= 2A_6 \frac{\zeta_\alpha}{U_n^*} - \frac{1}{\mu r_a^2} \left[(1 + 2a_h) A_7(1 - \psi_1 - \psi_2) + a_h \frac{b_n \tan \Lambda}{l} A_{10} \right] \\
 d_3 &= -\frac{1}{\mu r_a^2} \left[(1 + 2a_h) A_6(1 - \psi_1 - \psi_2) + (1 + 2a_h) \left(\frac{1}{2} - a_h \right) A_6(\psi_1 \varepsilon_1 + \psi_2 \varepsilon_2) + \frac{b_n \tan \Lambda}{l} (1 + 2a_h) \left(\frac{1}{2} - a_h \right) A_{11}(1 - \psi_1 - \psi_2) - \left(\frac{1}{2} - a_h \right) \frac{b_n \tan \Lambda}{l} A_{11} - \left(\frac{1}{8} + a_h^2 \right) \left(\frac{b_n \tan \Lambda}{l} \right)^2 A_{15} \right] \\
 d_4 &= -\frac{1}{\mu r_a^2} \left[(1 + 2a_h) \left(\frac{1}{2} - a_h \right) A_6(1 - \psi_1 - \psi_2) - \left(\frac{1}{2} - a_h \right) A_6 - \left(\frac{1}{8} + a_h^2 \right) \frac{2b_n \tan \Lambda}{l} A_{11} \right] \\
 d_5 &= \frac{1}{\mu r_a^2} \left[(1 + 2a_h) \psi_1 \varepsilon_1 \left(\varepsilon_1 A_7 - \frac{b_n \tan \Lambda}{l} A_{10} \right) \right] & d_6 &= \frac{1}{\mu r_a^2} \left[(1 + 2a_h) \psi_2 \varepsilon_2 \left(\varepsilon_2 A_7 - \frac{b_n \tan \Lambda}{l} A_{10} \right) \right]
 \end{aligned}$$

$$d_7 = -\frac{1}{\mu r_a^2} \left[(1 + 2a_h) \nu_1 \varepsilon_1 \left(A_6 \left(1 - \left(\frac{1}{2} - a_h \right) \varepsilon_1 \right) + \frac{b_n \tan \Lambda}{l} \left(\frac{1}{2} - a_h \right) A_{11} \right) \right]$$

$$d_8 = -\frac{1}{\mu r_a^2} \left[(1 + 2a_h) \nu_2 \varepsilon_2 \left(A_6 \left(1 - \left(\frac{1}{2} - a_h \right) \varepsilon_2 \right) + \frac{b_n \tan \Lambda}{l} \left(\frac{1}{2} - a_h \right) A_{11} \right) \right]$$

Appendix B

The coefficients of the Eqs. (18) and (22) are as follow

$$\begin{aligned}
 m_1 &= -c_b \omega^2 + c_3 + c_9 \varepsilon_1 t_1 + c_{10} \varepsilon_2 t_2 & m_2 &= c_4 \omega - c_9 \omega t_1 - c_{10} \omega t_2 & m_3 &= -d_b \omega^2 + d_3 + d_9 \varepsilon_1 t_1 + d_{10} \varepsilon_2 t_2 + \beta_\alpha (1/U^*)^2; \\
 m_4 &= d_4 \omega - d_9 \omega t_1 - d_{10} \omega t_2 & m_5 &= -e_b \omega^2 + e_3 + e_9 \varepsilon_1 t_1 + e_{10} \varepsilon_2 t_2 & m_6 &= e_4 \omega - e_9 \omega t_1 - e_{10} \omega t_2 \\
 p_1 &= -c_a \omega^2 + c_1 + c_7 \varepsilon_1 t_1 + c_8 \varepsilon_2 t_2 + \beta_\varepsilon (\Omega_1/U^*)^2 & p_2 &= c_2 \omega - c_7 \omega t_1 - c_8 \omega t_2 & p_3 &= -d_a \omega^2 + d_1 + d_7 \varepsilon_1 t_1 + d_8 \varepsilon_2 t_2 \\
 p_4 &= d_2 \omega - d_7 \omega t_1 - d_8 \omega t_2 & p_5 &= -e_a \omega^2 + e_1 + e_7 \varepsilon_1 t_1 + e_8 \varepsilon_2 t_2 & p_6 &= e_2 \omega - e_7 \omega t_1 - e_8 \omega t_2 \\
 q_1 &= -p_2, \quad q_2 = p_1 & q_3 &= -p_4, \quad q_4 = p_3 & q_5 &= -p_6, \quad q_6 = p_5 \\
 s_1 &= -c_c \omega^2 + c_5 + c_{11} \varepsilon_1 t_1 + c_{12} \varepsilon_2 t_2 & s_2 &= c_6 \omega - c_{11} \omega t_1 - c_{12} \omega t_2 & s_3 &= -d_c \omega^2 + d_5 + d_{11} \varepsilon_1 t_1 + d_{12} \varepsilon_2 t_2 \\
 s_4 &= d_6 \omega - d_{11} \omega t_1 - d_{12} \omega t_2 & s_5 &= -e_c \omega^2 + e_5 + e_{11} \varepsilon_1 t_1 + e_{12} \varepsilon_2 t_2 + \beta_\beta (\Omega_2/U^*)^2 & s_6 &= e_6 \omega - e_{11} \omega t_1 - e_{12} \omega t_2 \\
 u_1 &= -s_2, \quad u_2 = s_1 & u_3 &= -s_4, \quad u_4 = s_3 & u_5 &= -s_6, \quad u_6 = s_5 \\
 m_{13} &= -9c_b \omega^2 + c_3 + c_9 \varepsilon_1 t_{13} + c_{10} \varepsilon_2 t_{23} & m_{23} &= 3c_4 \omega - 3c_9 \omega t_{13} - 3c_{10} \omega t_{23} & m_{33} &= -9d_b \omega^2 + d_3 + d_9 \varepsilon_1 t_{13} + d_{10} \varepsilon_2 t_{23} + \beta_\alpha (1/U^*)^2 \\
 m_{43} &= 3d_4 \omega - 3d_9 \omega t_{13} - 3d_{10} \omega t_{23} & m_{53} &= -9e_b \omega^2 + e_3 + e_9 \varepsilon_1 t_{13} + e_{10} \varepsilon_2 t_{23} & m_{63} &= 3e_4 \omega - 3e_9 \omega t_{13} - 3e_{10} \omega t_{23} \\
 p_{13} &= -9c_a \omega^2 + c_1 + c_7 \varepsilon_1 t_{13} + c_8 \varepsilon_2 t_{23} + \beta_\varepsilon (\Omega_1/U^*)^2 & p_{23} &= 3c_2 \omega - 3c_7 \omega t_{13} - 3c_8 \omega t_{23} & p_{33} &= -9d_a \omega^2 + d_1 + d_7 \varepsilon_1 t_{13} + d_8 \varepsilon_2 t_{23} \\
 p_{43} &= 3d_2 \omega - 3d_7 \omega t_{13} - 3d_8 \omega t_{23} & p_{53} &= -9e_a \omega^2 + e_1 + e_7 \varepsilon_1 t_{13} + e_8 \varepsilon_2 t_{23} & p_{63} &= 3e_2 \omega - 3e_7 \omega t_{13} - 3e_8 \omega t_{23} \\
 v_{13} &= -m_{23}, \quad v_{23} = m_{13} & v_{33} &= -m_{43}, \quad v_{43} = m_{33} & v_{53} &= -m_{63}, \quad v_{63} = m_{53} \\
 q_{13} &= -p_{23}, \quad q_{23} = p_{13} & q_{33} &= -p_{43}, \quad q_{43} = p_{33} & q_{53} &= -p_{63}, \quad q_{63} = p_{53} \\
 s_{13} &= -9c_c \omega^2 + c_5 + c_{11} \varepsilon_1 t_{13} + c_{12} \varepsilon_2 t_{23} & s_{23} &= 3c_6 \omega - 3c_{11} \omega t_{13} - 3c_{12} \omega t_{23} & s_{33} &= -9d_c \omega^2 + d_5 + d_{11} \varepsilon_1 t_{13} + d_{12} \varepsilon_2 t_{23} \\
 s_{43} &= 3d_6 \omega - 3d_{11} \omega t_{13} - 3d_{12} \omega t_{23} & s_{53} &= -9e_c \omega^2 + e_5 + e_{11} \varepsilon_1 t_{13} + e_{12} \varepsilon_2 t_{23} + \beta_\beta (\Omega_2/U^*)^2 & s_{63} &= 3e_6 \omega - 3e_{11} \omega t_{13} - 3e_{12} \omega t_{23} \\
 u_{13} &= -s_{23}, \quad u_{23} = s_{13} & u_{33} &= -s_{43}, \quad u_{43} = s_{33} & u_{53} &= -s_{63}, \quad u_{63} = s_{53} \\
 t_1 &= (\varepsilon_1^2 + \omega^2)^{-1}, \quad t_{13} = (\varepsilon_1^2 + 9\omega^2)^{-1} & & & t_2 &= (\varepsilon_2^2 + \omega^2)^{-1}, \quad t_{23} = (\varepsilon_2^2 + 9\omega^2)^{-1}
 \end{aligned}$$